Studying monogenetic volcanoes with a Terrestrial Laser Scanner: Case study at Croscat volcano (Garrotxa Volcanic Field, Spain)

A. Geyer [(1)], D. García-Sellés[(2)], D. Pedrazzi[(1,3)], S. Barde-Cabusson[(1)], J. Marti [(1,)], J.A. Muñoz[(2)]

1. Group of Volcanology. SIMGEO (UB-CSIC). Institute of Earth Sciences Jaume Almera, ICTJA-CSIC, Lluis Sole i Sabaris s/n, 08028 Barcelona, Spain
2. Institut de Recerca Geomodels, Departament de Geodinàmica i Geofísica, Facultat de Geologia, Universitat de Barcelona (UB), Martí Franqués s/n, 08028 Barcelona, Spain
3. Centro de Geociencias, Universidad Nacional Autónoma de México, Campus Juriquilla, Querétaro, Qro. 76230, Mexico

corresponding author:

A. Geyer (ageyer@ictja.csic.es)

Tel: +34 934095410

Fax: +34 934110012

Abstract

Erosional processes (natural or anthropogenic) may partly destroy the relatively small-sized volcanic edifices characteristic of monogenetic volcanic zones, leaving their internal structure well exposed. Nevertheless, the study of these outcrops may be extremely challenging due to restricted accessibility or safety issues. Digital representations of the outcrop surface have been lately used to overcome such difficulties. Data acquired with Terrestrial Laser Scanning instruments using Light Detection And Ranging technology enables the construction of such digital outcrops. The obtained high-precision 3D terrain models are of greater coverage and accuracy than conventional methods and when taken at different times allow description of geological processes in time and space. Despite its intrinsic advantages and the proven satisfactory results, this technique has been little applied in volcanology-related studies. Here, we want to introduce it to the volcanological community together with a new and user-friendly digital outcrop analysis methodology for inexperienced users. This tool may be useful, not only for volcano monitoring purposes, but also to describe the internal structure of exposed volcanic edifices or to estimate outcrop erosion rates that may be helpful in terms of hazard assessment or preservation of volcanic landscapes. We apply it to the Croscat volcano, a monogenetic cone in the La Garrotxa Volcanic Field (Catalan Volcanic Zone, NE Spain), quarrying of which leads to a perfect view of its interior but restricts access to its uppermost parts. Croscat is additionally one of the most emblematic symbols of the La Garrotxa Volcanic Field Natural Park, and its preservation is a main target of the park administration.

Keywords

Terrestrial laser scanner, digital outcrop, Croscat volcano, La Garrotxa Volcanic Field, Catalan Volcanic Zone

1. Introduction

The specific eruption style of a monogenetic volcano is related to changes in magma composition (e.g. volatile content), magma supply rate and local tectonics. In addition, external environmental conditions at the moment of the eruption such as host rock geology, distribution and characteristics of the underlying aquifers also play a decisive role (e.g. Kokelaar 1986; Sohn and Chough 1989; Sohn 1996; White 1996; Walker 2000; White and Houghton 2000; Martí et al. 2011; Németh et al. 2011; White and Ross 2011; Pedrazzi et al. 2014). Therefore, a correct interpretation of the deposits and consequently, the reconstruction and characterization of the eruptive sequence is crucial to evaluate its potential hazard in the case of active areas (Fisher and Waters 1970; Heiken 1971; Lorenz 1973, 1986, 1987; Wohletz 1986).

Erosional processes (natural and/or anthropogenic) in a variety of settings may partly destroy these relatively small-sized volcanic edifices and expose their interiors (Fig. 1). For example, on volcanic islands, monogenetic volcanoes may occur in coastal plains where marine erosion may lead to an efficient demolishment of the constructed edifice (e.g. Volcano Capelinhos, Faial Island; Orakei Maar, Auckland Volcanic Field; El Golfo, Lanzarote Island) (Waters and Fisher 1971; Németh et al. 2012a; Pedrazzi et al. 2013) (Fig. 1a and b). Other natural mechanisms include river incision as in the case, for example, of Los Loros volcano (Mendoza, Argentina) (Németh et al. 2012b). Furthermore, monogenetic volcanic edifices close to populated areas tend to be a common target for quarrying since the extracted material is often used for construction and decoration purposes, as has occurred with the Croscat volcano (Garrotxa Volcanic Field, Spain) (Fig. 1c). Thus, when working on monogenetic volcanic areas it is usual to find outcrops where the internal structure of the edifices is, for one or other reason, well exposed. However, their study may be sometimes extremely difficult (or even impossible) due the lack of accessibility or safety issues.

In the few last years, digital (or virtual) outcrops have made possible the study of those areas with natural access limitations or safety issues (e.g. Dueholm and Olsen 1993; Xu et al. 2000; Adams et al. 2005; McCaffrey et al. 2005; Jones et al. 2009). Furthermore, these digital representations of the outcrop surface may facilitate visualization of the interesting structures, as long as they can be analysed while navigated in real-time, with optional displays for perspective, scale distortions, and attribute filtering, etc. (cf. García-Sellés et al. 2011).

In particular, Terrestrial Laser Scanning (TLS) instruments using Light Detection And Ranging technology (LIDAR) are capable of capturing topographic details and achieve modelling accuracy within a few centimetres. The data obtained, called a Point Cloud, enables the creation of detailed 3-D terrain models of greater coverage and accuracy than conventional methods and with almost complete safety of the operators (Jones 2006).

Recently, such high-precision digital surface models have played an important role in the study of glacier evolution (Conforti et al. 2005), gravitational instabilities (Abellan et al. 2010), landslides (Jones 2006; Jaboyedoff et al. 2012), and tectonic deformation (Nissen et al. 2012). High-precision digital surface models captured at different times may be compared, allowing description of geological processes in time and space. In some cases, this enables their detection and spatial prediction of occurrence in the future (Abellan et al. 2010; Jaboyedoff et al. 2012). It can also be used to estimate deformation patterns, displacements, surface variations, volumes involved in mass movements, and other physical features (e.g. Kaab and Funk 1999; Baldi et al.

2000; Mora et al. 2003; van Westen and Lulie Getahun 2003; Pesci et al. 2004; Nissen et al. 2012).

Airborne LIDAR technology has already been extensively applied in volcanology for precise mapping, accurate morphometric and volumetric measurement of surface features such as lava flows and domes, and estimating differential erosion in river valleys (e.g. Crow et al. 2008; Ventura and Vilardo 2008; Favalli et al. 2009, 2010; Procter et al. 2010). Nonetheless, despite its intrinsic advantages for studying inaccessible outcrops and the proven satisfactory results, the TLS technique has just been applied in a few volcanology-related studies. To the authors' knowledge it has been mainly used for volcano monitoring and hazard assessment purposes on Mt. Etna (Hunter et al. 2003; James et al. 2009; Marsella et al. 2011) and Soufriere Hills (Jones 2007); to accurately map the inaccessible surfaces of Vesuvius (Conforti et al. 2006; Pesci et al. 2007) and Mt. Ruapehu craters (Massey et al. 2010) and to reconstruct flood basalt lava flows from outcrop data in the Faroe Islands and the Isle of Skye (Nelson et al. 2011).

The aim of the present paper is to introduce TLS and the potential use of the obtained data to the volcanological community. We show here how the acquired and processed data may be useful, not only for volcano monitoring purposes, but also to describe the exposed internal structure of volcanic edifices or to estimate erosion rates that may be helpful in terms of hazard assessment or preservation of volcanic landscapes. We also present a new and user-friendly methodology to extract geological data from digital outcrops, specifically aimed at inexperienced TLS users. This new technique works in a simple environment and is mainly based on digitized images, a tool well known by geoscientists. The main advantage of this new method is that the digitized outcrop images are converted to realistic 3D images in a referenced coordinate system, where measurements and other analyses can be performed.

We use as an example of application the Croscat volcano, a monogenetic volcanic cone of La Garrotxa Volcanic Field (Spain) (Fig.1c). Commercial quarrying until 1991 exposed the internal part of the volcano but made access difficult to the uppermost parts. Croscat volcano is in addition a symbol of the La Garrotxa Volcanic Field Natural Park; its preservation is a main target of the park administration. Thus, studying and evaluating its degradation due to external processes such as heavy rains or snowfalls is an indispensable task for ensuring its correct preservation.

2. Terrestrial Laser Scanner

2.1 Terrestrial Laser Scanner: An overview

The TLS is an efficient topographical survey instrumentation used to acquire a redundant number of points distributed over a physical surface (Fig. 2a). The operating methodology of this technique consists of measuring the time it takes a laser pulse to travel from the transmitter to the remote target be reflected and return to the system receiver (Fig. 2a). A high-speed counter measures the time of flight t from the start pulse to the return pulse, which is converted to a distance d as follows (Petrie and Toth 2008a, 2008b):

$$d = \frac{(c \times t\,)}{2} \qquad [1]$$

where c is the speed of light.

The relative coordinates of each measurement point i with respect to the location of the TLS device are obtained from the orientation angles of each pulse and the distance d_i. TLS devices are able to collect, with high accuracy, millions of points in a few minutes. Most outdoor geological applications of TLS use the time-of-flight technique, due to the scale and the range of the objects to be captured (from tens to hundreds of meters). For example, the TLS used here reaches a point accuracy of 0.8 cm at a range of 90 m for 70% of the captured points (technical specifications supplied by Optech Company). Discussion of TLS principles and other technical details is beyond the scope of this paper, but it can be found in Teza et al. (2007), while Buckley et al. (2008) present a useful discussion on the accuracy of TLS and related outputs.

2.2 TLS Equipment

The TLS (ground-based LIDAR) used here is the ILRIS 3D model from the Optech Inc. Company. It consists of a transmitter/receiver of infrared laser pulses (1,535 nm wavelength) and a scanning device. For the present work, the TLS is programmed to record the first pulse return since it minimise the ambiguities when classifying the nature of the reflected object. In most cases, recording the last pulse does not guarantee that this comes directly reflected from the ground. In ideal conditions, depending on the scanned surface reflectivity and visibility, this scanner can register pulses from objects at distances up to 1,000 m. The most satisfactory density of returned pulses is obtained for objects $\leqslant$ 500 m from the receiver.

The TLS is equipped with a laptop or palm computer, which acts as the interface, and a power supply (e.g. batteries or generator). The TLS used here was also set up with a differential GPS and an external Single Lens Reflex digital camera (Fig. 2b). The equipment package has to be kept light for portability and to enable rapid field deployment.

2.3 Data acquisition and processing

To minimise errors and ensure good outcrop coverage, it is necessary to scan from different view-points, also called stations. The resultant point clouds are subsequently aligned and merged into a single reference system by specific TLS software like PolyWorks (http://www.innovmetric.com) or RiScanPro (http://www.riegl.com). Alignment is based on the supervised identification of overlapping zones and their successive merging by algorithms using least-squares surfaces matching or iterative closest points (Besl and McKay 1992; Gruen and Akca 2005). In this work, in order to construct a final 3D model, obtained data has been processed with the PolyWorks *IMAlign Module*. The mean point spacing of the acquired datasets ranges from 3 to 5 cm up to a maximum range of 290 m. The *IMAlign Module* constructs a surface model for image scans with cells of 5 cm to match the different scans.

Once the individual point clouds have been aligned into the same reference system, the diverse TLS stations are also incorporated. Since we have also captured GPS data of the latter individual view-points during the field survey, we are able to georeference the final point cloud and orientate it towards the geographic North. This procedure provides the TLS positioning with sub-decimetric error. In this case study we use the Universal Transverse Mercator (UTM) coordinate system (Datum ED50).

Finally, we convert the georeferenced 3D point cloud into a photo-realistic model of the entire outcrop by overlying the digital images taken simultaneously with the scans on the terrain surface (Fig. 2c). Since the digital camera moves with the TLS, the perspective of the captured image is almost perpendicular in all cases, i.e. distortion is reduced.

2.4 Studying geological outcrops with TLS

Traditionally, the most common practice in geological outcrop studies starting from an outcrop point cloud or photo-textured surfaces has been the following (García-Sellés et al. 2011): (1) interpretation of geological surfaces by visual inspection of the point cloud or the photo-textured surface, completed by manual digitisation (Trinks et al. 2006; Fabuel-Perez et al. 2009), (2) interpolation or extrapolation of the geological surfaces by using the digitized contacts as input constraints (Xu et al. 2000); and (3) reconstruction of the surfaces from the outcrop to use them as a framework to build and populate 3D geocellular models (Hodgetts et al. 2004; Pringle et al. 2004; Bellian et al. 2005; Enge et al. 2007; Fabuel-Perez et al. 2009).

Here, we present a new methodology to enable inexperienced TLS users to extract data from the obtained 3D point cloud. For this, we exploit the broad experience of geoscientists in working with 2D digitized images. The newly developed DigiStruc-3D software is an easy to use technique that projects a geologic feature detected in the 2D digital (or digitized) images onto the point cloud and extracts the objects in 3D (Fig. 2c). DigiStruc-3D software is available from GEOMODELS Research Institute (http://www.ub.edu/geomodels/index.html) upon request.

For this, we use the well known methodology applied in photogrammetric studies, which relates reference systems of the image and the point cloud captured by the Single Lens Reflex digital camera and TLS, respectively (Wong 1980). Since our camera is coupled to the TLS device, required parameters such as position, orientation, focal length, and lens distortion are constant or easy to calculate. Thus, for each point digitized on the 2D image, we are able to assign a 3D point cloud coordinate. Applying the collinearity equation (i.e. property of a set of point of lying on a single line), from digitized lineations recognized in the 2D images (Figs. 2c and 3 label I), which are the geometric result of the intersection between the surface outcrop and diverse geological planes, we are able to extract parameters like the orientation and trace length from this surface (Fig. 3 label II).

In a second step, for each pair of nodes digitized over the 2D image and projected over the point cloud, the algorithm interpolates points between the two nodes to increment the number of data points. This allows better accuracy in the geometric measurements associated with the object. As soon as the user ends digitizing a line or polygon our algorithm calculates a planar regression with the selected 3D points and calculates the normal vector.

The above described methodology allows us to obtain a set of 3D digital objects whose position, length and orientation can be measured, allowing the spatial relation between objects to be more efficiently studied. Furthermore, it is possible to use the obtained 3D structures that may represent stratigraphic bodies, faults, joints, bedding, etc., as input data for detailed numerical models.

3. Application to Croscat volcano

3.1 Background

Croscat volcano is located in La Garrotxa Volcanic Field, part of the Catalan Volcanic Zone (CVZ) in the NE Iberian Peninsula (Fig. 4a) (Martí et al. 2011; Pedrazzi et al. 2014). The CVZ hosts the greatest concentration of Middle Miocene to recent volcanism in the region and is related to the period of extensional tectonics and mafic alkaline volcanism of the Neogene Valencia Trough (Martí et al. 1992) (Fig. 4a).

Croscat volcano is one of the most representative edifices of the northern sector of La Garrotxa Volcanic Field and was constructed during the same fissure-fed eruption that formed the Santa Margarida and La Pomareda volcanoes, all lying on a 3 km long eruption fissure oriented NNW–SSE (Fig. 5) (Martí et al 2011).

The Croscat succession has been studied by Di Traglia et al. (2009), Cimarelli et al., (2010), Martí et al. (2011) and Bolós et al. (2014) and the reader is referred to these works for further details on its stratigraphy and eruptive sequence. Construction of the Croscat scoria cone started immediately after a phreatomagmatic explosive episode that formed the Santa Margarida crater (PS1 in Fig. 6). The first cone-building deposits of Croscat and La Pomareda comprise massive basaltic spatter and welded scoria agglomerates deposited as the eruption progressed along the fissure (SS in Fig. 6). Later on, the eruption concentrated in the central part of the fissure, changing from fissural to a central conduit (Strombolian phase), completing construction of the Croscat scoria cone (Martí et al. 2011). This Strombolian activity generated two main scoria fallout units. The lower one is a thick, poorly stratified coarse lapilli size scoria deposit with several scoria bomb beds (SLB in Fig. 6). The upper unit consists of more than ten meters of well stratified to thinly laminated, medium to fine lapilli size scoria, which contains sparse scoria bombs and blocks (SL in Fig. 6). At the top of the pyroclastic succession, the eruption changed from Strombolian to phreatomagmatic generating a widespread pyroclastic surge deposit (PS2 in Fig. 6) (Martí et al. 2011). The last eruptive phase of Croscat corresponded to a lava flow, whose emplacement caused the breaching of the western flank of the cone (Fig. 5b).

3.2 Studying Croscat volcano with TLS

The studied outcrop (Fig. 6) is the result of the commercial quarrying of Croscat volcano carried out until 1991, making the place unique for studying and admiring the internal parts of the volcanic edifice but also highly vulnerable to erosion processes. On March 2012, we carried out a TLS survey consisting of eight, partially overlapped, single scans totalling up to 14.5 million georeferenced points. These scans were acquired from three different positions (Fig. 7a, S1-S3) and subsequently merged into a single reference system (Fig. 7b). The collected information is used to: i) evaluate the degradation of the outcrop in the last few years due to natural erosional processes; and ii) to study the internal structure of the volcanic cone.

3.2.1 Estimating outcrop erosion

One direct result obtained after processing TLS acquired data is a high resolution Digital Elevation Model (DEM) of the scanned area. For example, in the case of Pesci et al. (2007), they generated a triangulated model of the Vesuvius volcano crater with a mean cell size of 5 cm. Such high-resolution DEMs are useful for both individual surface analysis or, by comparing with previous DEMs, estimating morphological variations, physical surface changes and mass movement. In our case, with the data acquired in the March 2012 TLS survey we developed a DEM of the Croscat outcrop with a resolution of up to 1 point each 4-5 cm, covering an area of 300 $\times$ 150 meters.

This DEM, quickly obtained with a single TLS survey, allowed a first order estimate of the outcrop erosion due to continuous and, in most cases, heavy rainfalls that occurred during 2010 and 2011. As illustrated in Figure 8, during this time period the area experienced the wettest months and the heaviest rainfalls of the last 9 years (Fig. 8). The total amount of accumulated rain during these years was also considerably higher compared with previous years or the mean total annual rain for the period 2003-2012 (Fig. 8b). Additionally, field observations revealed some morphological variation at the upper part of the outcrop, indicating that natural erosion could be accelerated due to these periods of anomalous heavy rainfalls.

In order to evaluate the amount of erosion that occurred, we compared the DEM obtained with the TLS survey (DEM_{TLS}) with the previous 2×2m resolution model provided by the Institut Cartográfic i Geològic de Catalunya ICGC (Catalan Cartographic and Geologic Institute, http://www.icc.cat) (DEM_{ICGC}). The data source of the DEM_{ICGC} corresponds to the points obtained during an airborne LiDAR survey conducted in early 2010, which recorded signal from multiple returns, canopy, branches and ground. According to the technical notes of the ICGC, the mean square error of the obtained data is 0.15m. In order to elaborate the DEM_{ICGC} we use either the last recorded signal or, if this is of bad quality, the canopy signal subtracting a mean tree height. In this second case, the mean value chosen would not affect the DEM_{ICGC} values along the talus. Results obtained are illustrated in Figure 9. Note that we calculated DEM_{TLS}- DEM_{ICGC}, i.e. negative difference values indicate a decrease in topographic height (erosion) during the period 2010-2012. From the general differences map hardly any changes are observable on the talus area (Fig. 9a). The maximum positive and negative values are concentrated at the uppermost outcrop wall (Fig. 9a label I) and around the outcrop (Fig. 9a label II), respectively. The latter are due to the presence of vegetation (e.g. trees and bushes). Whereas the DEM_{ICGC} is filtered (i.e. vegetation is removed from the obtained elevation data), our DEM_{TLS} includes them. Therefore, the "increase" in topography in these areas reflects the inclusion of vegetation, with the greatest differences corresponding to the highest trees. The negative values along the uppermost southeast wall (Fig. 9a label II), i.e. topography "decrease" between 2010 and 2012, may partly represent erosion of the outcrop wall during this time period.

Focusing on the talus area (Fig. 9b), we observe at the upper parts negative differences indicating significant erosion (up to 0.5 m). Material eroded from the outcrop walls (Fig. 9b label III) would have accumulated parallel to the maximum slope lines of the talus indicated by the positive DEM_{TLS}- DEM_{ICGC} values (Fig. 9b label IV). A total volume of c. 450 m^3 of material has been eroded from the uppermost parts of the outcrop and vertical cliffs and accumulated in the talus area during the period 2010-early March 2012.

In order to minimize the error implicit in using two digital elevation models of different resolution, we resampled and aligned both DEMs. Nevertheless, problems appear in cliffs and abrupt slopes, where DEM_{TLS} and DEM_{ICGC} approximate the topography at a centimetre or metre scale, respectively. A detailed study of the erosional processes occurring at the outcrop is beyond the scope of this paper, and thus only a first order estimate is provided here. In the future, if this becomes the main objective, a more accurate analysis of erosion and accumulation rates and general degradation patterns should consider repeated detailed TLS surveys of the outcrop.

3.2.2 Analysis of the Croscat internal structure

A further application of the TLS data is in studying the internal structure of the volcanic edifice and determining, for example, the slope angle of the edifice during the different eruptive stages. This is especially useful when dealing with inaccessible outcrops, as is the case for the upper parts of the outcrop under study. For this, we applied the methodology described in section 2.4. We used our 3D photo-realistic model of the outcrop and previous knowledge of the volcano stratigraphy (if available) to identify the most visible contacts between the different depositional units and individual layers (Fig. 10). Once the structures were marked, the DigiStruc-3D program allows us to extract information concerning the strike and dip of the marked planes (Fig. 3) and hence the 3D reconstruction of the identified structures (Fig. 11).

The morphology of cinder cones is mainly governed by the eruption rate, the accumulation rate around the vent, and the grain-size distribution of ejected pyroclasts. The resultant slope angles range between 10 and 35° and are mainly controlled by the angle of repose of the scoria. The latter vary slightly with grain size, shape, rheology and wetness, as well as climatic factors (Barabási et al. 1999; Robinson and Friedman 2002; Riedel et al. 2003; Bemis et al. 2011). Results obtained here indicate how the slope angle of the cone changes from around 17° in the lower units to up to ~30° in the upper parts. These values provide a first order estimate of the growth rate of the edifice, which is strongly dependent on the eruption mechanisms observed for Strombolian-type eruptions (e.g. McGetchin et al. 1974; Settle 1979) or column-forming eruptions similar to Plinian eruptions (e.g. Riedel et al. 2003). These different mechanisms may have a strong influence on grain size and fragmentation, affecting the proportion of the magma that ends up on the cinder cone since the size and growth of a cone are the result of the amount of magma erupted less the amount transported into the buoyant volcanic plume.

5. Discussion and conclusions

TLS has been repeatedly applied in the last years for the study of natural processes such as landslides, rock mass movements, glacier retreat, etc. Since high-resolution measurements can be taken from distances up to hundreds of meters, it has become a useful tool for characterization and monitoring of inaccessible outcrops or those with unstable slopes or in cliffs. It has also been considered an innovative and promising instrument for panoramic view surveys.

TLS allowed us to determine the volume of material eroded from the Croscat volcano quarry in nearly two years. The major factor likely responsible for erosion in our case-study outcrop are anomalous heavy rainfalls that occurred between acquisition of the two DEMs (Fig. 8c and d). Nevertheless, additional erosion factors may be involved here and in other contexts (e.g. wind, cryofracturing, seismic events, etc.). Only surveys repeated several times in a year or, ideally, real-time monitoring could help quantify the relative roles of episodic/catastrophic events versus sustained erosive processes in the total erosion rate.

The advantages of obtaining digital outcrops are not only restricted to solving accessibility issues. The study of digital outcrops may facilitate visualization of the features of interest over the entire outcrop, as long as the digital outcrop can be analysed and navigated in real- time, with optional displays for perspective, scale distortions, and attribute filtering. The main advantages of the technique are the acquisition of real 3D information, fast data capture accurate measurement of distance, offset between layers or angles and dips, easy set up and portability and its high resolution, at least for the ground-based instrument. Conversely, the main limitations of the ground-based technique are the existence of shadow areas caused by rugged topography, the huge quantity of acquired information and the need for post-processing to filter and align data sets, i.e. when a large area is scanned, several data sets must be merged and due to error propagation the alignment starts to be more complicated and time-consuming to obtain reliable results.

TLS and Digistruc-3D software allowed us to reconstruct stratigraphic planes, and in particular those corresponding to the transition from one eruptive phase to another. Acquisition of TLS data at several outcrops around a volcanic edifice may thus contribute to stratigraphic studies that allow estimates of the volumes of magma erupted during each eruptive phase that was not dispersed beyond the cone perimeter. We were not able to test this idea for Croscat because of the vegetation covering the rest of the cone but this would theoretically enable reconstruction of a 3D view of the interior of a volcano. The more complex the eruptive history of a volcano the less accurate will be volume estimation. Monogenetic volcanoes would therefore be better candidates for such studies than larger edifices.

Despite its evident advantages and ability to construct high-resolution digital outcrops, the application of the TLS technique to volcanology–related processes or studies has been quite restricted. The outstanding results by Pesci et al. (2007) confirmed that this laser scanner methodology is perfectly suitable for applications in volcanic areas. In their work, they completely scanned the crater of Vesuvius in few hours; data processing producing a DEM model with a mean grid size of 5 cm. Furthermore, by comparing high-resolution models from different surveys, it is possible to rapidly estimate morphological variations, surface changes and mass movement, making this technique a quite efficient system for volcano monitoring.

Indeed, TLS portability and ability to operate remotely without accessing dangerous areas is a crucial feature and an advantage for work in remote areas or in volcanically active zones. The short data acquisition time reduces the exposure time of the operators in potentially dangerous areas such as active volcanic craters (Jones 2006; Massey et al. 2010).

Here, we have shown how Terrestrial Laser Scanning surveys currently represent one of the most powerful tools to accurately map inaccessible surfaces with very short survey time. The obtained georeferenced point cloud can be used for multiple purposes including the generation of high-resolution digital elevation models. The latter may be useful to determine and evaluate erosion patterns, or combined with the digital images to extract 3D information of the stratigraphic units.

6. Acknowledgements

We thank the Natural Park of the La Garrotxa Volcanic Field and its staff for permission to undertake this research and for all their support we have always received from them. AG is grateful for her Juan de la Cierva post-doctoral grant (JCI-2010-06092) and her Ramón y Cajal contract (RYC-2012-11024). SBC acknowledges the JAE-Doc postdoctoral personal grant program of CSIC (JAEDoc_09_01319). This work was partly financed by projects CGL2010-21968-C02-01,CGL2010-18609 and CGL2013-40828-R of the Spanish Ministry of Science and Innovation. The editor Vern Manville and the reviewers Gabor Kereszturi and Laurent Michon are thanked for their thorough and constructive reviews, which resulted in substantial improvements to this paper.

7. References

Abellan A, Calvet J, Vilaplana JM, Blanchard J (2010) Detection and spatial prediction of rockfalls by means of terrestrial laser scanner monitoring. Geomorphology **119**:*162-171*

Adams EW, Grotzinger JP, Waters WA, Schroder S, McCormick D, Al-Siyabi H (2005) Digital characterization of thrombolite–stromatolite reef distribution in a carbonate ramp system (terminal Proterozoic, Nama Group, Namibia). American Association of Petroleum Geologists Bulletin **89**:*1293-1318*

Baldi P, Bonvalot S, Briole P, Marsella M (2000) Digital photogrammetry and kinematic GPS applied to the monitoring of Vulcano Island, Aeolian Arc, Italy. Geophysical Journal International **142**(3):*801-811*

Barabási A-L, Albert R, Schiffer P (1999) The physics of sand castles: maximum angle of stability in wet and dry granular media. Physica A: Statistical Mechanics and its Applications **266**(1-4):*366-371*

Bellian JA, Kerans C, Jennette DC (2005) Digital outcrop models: applications of terrestrial scanning LIDAR technology in stratigraphic modelling. Journal of Sedimentary Research **72**:*166-176*

Bemis K, Walker J, Borgia A, Turrin B, Neri M, Swisher Iii C (2011) The growth and erosion of cinder cones in Guatemala and El Salvador: Models and statistics. Journal of Volcanology and Geothermal Research **201**(1-4):*39-52*

Besl PJ, McKay ND (1992) A Method for Registration of 3-D Shapes. IEEE Transactions on Pattern Analysis and Machine Intelligence **14**(2):*239-256*

Bolós X, Planagumà L, Martí J (2014) Volcanic stratigraphy of the Quaternary La Garrotxa Volcanic Field (north-east Iberian Peninsula). Journal of Quaternary Science **29**(6):*547-560*

Buckley SJ, Howell JA, Enge HD, Kurz TH (2008) Terrestrial laser scanning in geology: data acquisition, processing and accuracy considerations. Journal of the Geological Society **165**(3):*625-638*

Cimarelli C, Di Traglia F, Taddeucci J (2010) Basaltic scoria textures from a zoned conduit as precursors to violent Strombolian activity. Geology **38**(5):*439-442*

Conforti C, DEline P, Mortara G, Tamburini A (2005) Terrestrial Scanning LiDAR Technology applied to study the evolution of the ice-contact image lake (Mont Blanc, Italy). In: Proceedings of the 9th Alpine Glaciological Meeting. Milan, Italy

Conforti D, Pesci A, Fabris M, Loddo F, Anzidei M, Baldi P, Pingue F, Pinto L (2006) Terrestrial lidar (laser) scanner technology applied to survey the Vesuvio volcano (Italy) for geological and geo-morphological analysis. In: European Geosciences Union. Geophysical Research Abstracts, Vienna, Austria, p 08236

Crow R, Karlstrom KE, McIntosh W, Peters L, Dunbar N (2008) History of Quaternary volcanism and lava dams in western Grand Canyon based on lidar analysis, ^{40}Ar/^{39}Ar dating, and field studies: Implications for flow stratigraphy, timing of volcanic events, and lava dams. Geosphere **4**(1):*183-206*

Di Traglia F, Cimarelli C, de Rita D, Gimeno Torrente D (2009) Changing eruptive styles in basaltic explosive volcanism: Examples from Croscat complex scoria cone, Garrotxa Volcanic Field (NE Iberian Peninsula). Journal of Volcanology and Geothermal Research **180**(2-4):*89-109*

Dueholm KS, Olsen T (1993) Reservoir analog studies using multimodel photogrammetry: a new tool for the petroleum industry. American Association of Petroleum Geologists Bulletin **77**:*2023-2031*

Enge HD, Buckley SJ, Rotevatn A, Howell J (2007) From outcrop to reservoir simulation model: workflow and procedures. Geosphere **3**:*469-490*

Fabuel-Perez I, Hodgetts D, Redfern J (2009) A new approach for outcrop characterization and geostatistic analysis of a low-sinuosity fluvial-dominated succession using digital outcrop models: upper Triassic Oukaimeden Sandstone Formation, central High Atlas, Morocco. American Association of Petroleum Geologists Bulletin **93**:*795-827*

Favalli M, Karátson Dv, Mazzarini F, Pareschi MT, Boschi E (2009) Morphometry of scoria cones located on a volcano flank: A case study from Mt. Etna (Italy), based on high-resolution LiDAR data. Journal of Volcanology and Geothermal Research **186**(3-4):*320-330*

Favalli M, Fornaciai A, Mazzarini F, Harris A, Neri M, Behncke B, Pareschi MT, Tarquini S, Boschi E (2010) Evolution of an active lava flow field using a multitemporal LIDAR acquisition. Journal of Geophysical Research: Solid Earth **115**(B11):*B11203*

Fisher RV, Waters AC (1970) Base surge bed forms in Maar volcanoes. American Journal of Science **268**:*157-180*

García-Sellés D, Falivene O, Arbués P, Gratacos O, Tavani S, Muñoz JA (2011) Supervised identification and reconstruction of near-planar geological surfaces from terrestrial laser scanning. Computers & Geosciences **37**(10):*1584-1594*

Gruen A, Akca D (2005) Least squares 3D surface and curve matching. ISPRS Journal of Photogrammetry and Remote Sensing **59**(3):*151-174*

Guérin G, Behamoun G, Mallarach JM (1985) Un exemple de fusió parcial en medi continental. El vulcanisme quaternari de la Garrotxa. Publicació del Museu Comarcal de la Garrotxa, Vitrina:*19-26*

Heiken GH (1971) Tuff Rings: Examples from the Fort Rock-Christmas Lake Valley Basin, South-Central Oregon. Journal of Geophysical Research **76**(23):*5615-5626*

Hunter G, Pinkerton H, Airey R, Calvari S (2003) The application of a long-range laser scanner for monitoring volcanic activity on Mount Etna. Journal of Volcanology and Geothermal Research **123**(1-2):*203-210*

Jaboyedoff M, Oppikofer T, Abellan A, Derron M-H, Loye A, Metzger R, Pedrazzini A (2012) Use of LIDAR in landslide investigations: a review. Natural Hazards **61**:*5-28*

James MR, Pinkerton H, Applegarth LJ (2009) Detecting the development of active lava flow fields with a very-long-range terrestrial laser scanner and thermal imagery. Geophysical Research Letters **36**(22):*L22305*

Jones LD (2006) Monitoring landslides in hazardous terrain using terrestrial LiDAR: an example from Montserrat. Quarterly Journal of Engineering Geology and Hydrogeology **39**(4):*371-373*

Jones LD (2007) The application of terrestrial lidar to volcano monitoring – an example from the Montserrat Volcano Observatory. Civil Engineering Surveyor **November**:*21-23*

Jones RR, McCaffrey KJW, Clegg P, Wilson RW, Holliman NS, Holdsworth RE, Imber J, Waggot S (2009) Integration of regional to outcrop digital data: 3D visualization of multi-scale geological models. Computer and Geosciences **35**:*4-18*

Kaab A, Funk A (1999) Modelling mass balance using photogrammetric and geophysical data: A pilot study at Griesgletscher, Swiss Alps. Journal of Glaciology **45**:*575-583*

Kokelaar P (1986) Magma-water interactions in subaquous and emergent basaltic volcanism. Bulletin of Volcanology **48**:*275-289*

Lorenz V (1973) On the formation of maars. Bulletin of Volcanology **37**:*183-204*

Lorenz V (1986) On the growth of maars and diatremes and its relevance to the formation of tuff rings. Bulletin of Volcanology **48**:*256-274*

Lorenz V (1987) Phreatomagmatism and its relevance. Chemical Geology **62**:*149-156*

Martí J, Mitjavila J, Roca E, Aparicio A (1992) Cenozoic magmatism of the Valencia trough (western Mediterranean): relationship between structural evolution and volcanism. Tectonophysics **203**:*145-165*

Martí J, Planagumà L, Geyer A, Canal E, Pedrazzi D (2011) Complex interaction between Strombolian and phreatomagmatic eruptions in the Quaternary monogenetic volcanism of the Catalan Volcanic Zone (NE of Spain). Journal of Volcanology and Geothermal Research **201**(1-4):*178-193*

Marsella M, Scifoni S, Coltelli M, Proietti C (2011) Quantitative analysis of the 1981 and 2001 Etna flank eruptions: a contribution for future hazard evaluation and mitigation. Annals of Geophysics **54**(5)

Massey C, Manville V, Hancox G, Keys H, Lawrence C, McSaveney M (2010) Out-burst flood (lahar) triggered by retrogressive landsliding, 18 March 2007 at Mt Ruapehu, New Zealand,-a successful early warning. Landslides **7**(3):*303-315*

McCaffrey KJW, Jones RR, Holdsworth RE, Wilson RW, Clegg P, Imber J, Holliman N, Trinks I (2005) Unlocking the spatial dimension: digital technologies and the future of geoscience fieldwork. Journal of the Geological Society **162**:*927-938*

McGetchin TR, Settle M, Chouet BA (1974) Cinder cone growth modeled after Northeast Crater, Mount Etna, Sicily. Journal of Geophysical Research **79**(23):*3257-3272*

Mora P, Baldi P, Casula G, Fabris M, Ghirotti M, Mazzini E, Pesci A (2003) Global Positioning Systems and digital photogrammetry for the monitoring of mass movements: application to the Ca' di Malta landslide (northern Apennines, Italy). Engineering Geology **68**(1-2):*103-121*

Nelson CE, Jerram DA, Hobbs RW, Terrington R, Kessler H (2011) Reconstructing flood basalt lava flows in three dimensions using terrestrial laser scanning. Geosphere **7**(1):*87-96*

Németh K, Haller MJ, Siebe C (2011) Maars and scoria cones: the enigma of monogenetic volcanic fields. Journal of Volcanology and Geothermal Research **201**(1-4): *v-viii*

Németh, K., Agustin-Flores, J., Briggs, R., Cronin, S.J., Kereszturi, G., Lindsay, J.M., Pittari, A. and Smith, I.E.M. (2012a). Monogenetic volcanism of the South Auckland and Auckland Volcanic Fields IAVCEI - CMV/CVS - IAS Fourth International Maar Conference: A Multidisciplinary Congress on Monogenetic Volcanism [20 – 24 February 2012]. Geoscience Society of New Zealand Miscellaneous Publication, Auckland, New Zealand.

Németh K, Risso C, Nullo F, Smith IEM, Pécskay Z (2012b) Facies architecture of an isolated long-lived, nested polygenetic silicic tuff ring erupted in a braided river system: The Los Loros volcano, Mendoza, Argentina. Journal of Volcanology and Geothermal Research **239-240**(0):*33-48*

Nissen E, Krishnan AK, Arrowsmith JR, Saripalli S (2012) Three-dimensional surface displacements and rotations from differencing pre- and post-earthquake LiDAR point clouds. Geophysical Research Letters **39**(16): *L16301*

Pedrazzi D, Martí J, Geyer A (2013) Stratigraphy, sedimentology and eruptive mechanisms in the tuff cone of El Golfo (Lanzarote, Canary Islands). Bulletin of Volcanology 75:1-17 doi:10.1007/s00445-013-0740-3

Pedrazzi D, Bolós X, Martí J (2014) Phreatomagmatic volcanism in complex hydrogeological environments: La Crosa de Sant Dalmai maar (Catalan Volcanic Zone, NE Spain). Geosphere **10**(1): 170-184

Pesci A, Baldi P, Bedin A, Casula G, Cenni N, Fabris M, Loddo F, Mora P, Bacchetti M (2004) Digital elevation models for landslide evolution monitoring: application on two areas located in the Reno River Valley (Italy). Annals of Geophysics **47**:*1339-1353*

Pesci A, Loddo F, Conforti C (2007) The first terrestrial laser scanner application over Vesuvius: High resolution model of a volcano crater. International Journal of Remote Sensing **28**(1):*203-219*

Petrie G, Toth CK (2008a) I. Introduction to laser ranging, profiling and scanning. In: Shan J, Toth CK (eds) Topographic laser ranging and scanning: principles and processing. CRC Press, Taylor & Francis

Petrie G, Toth CK (2008b) III. Terrestrial laser scanners. In: Shan J, Toth CK (eds) Topographic laser ranging and scanning: principles and processing. CRC Press, Taylor & Francis

Pringle JK, Westerman AR, Clark JD, Drinkwater NJ, Gardiner AR (2004) 3D high-resolution digital models of outcrop analogue study sites to constrain reservoir model uncertainty: an example from Alport Castles, Derbyshire, UK. Petroleum Geoscience **10**:*343-352*

Procter J, Cronin SJ, Fuller IC, Lube G, Manville V (2010) Quantifying the geomorphic impacts of a lake-breakout lahar, Mount Ruapehu, New Zealand. Geology **38**(1):*67-70*

Riedel C, Ernst GGJ, Riley M (2003) Controls on the growth and geometry of pyroclastic constructs. Journal of Volcanology and Geothermal Research **127**(1-2):*121-152*

Robinson DA, Friedman SP (2002) Observations of the effects of particle shape and particle size distribution on avalanching of granular media. Physica A: Statistical Mechanics and its Applications **311**(1-2):*97-110*

Settle M (1979) Formation and deposition of volcanic sulfate aerosols on Mars. Journal of Geophysical Research: Solid Earth **84**(B14):*8343-8354*

Sohn YK (1996) Hydrovolcanic processes forming basaltic tuff rings and cones on Cheju Island, Korea. Geological Society of America Bulletin **108**(10):*1199-1211*

Sohn YK, Chough SK (1989) Depositional processes of the Suwolbong tuff ring, Cheju Island (Korea). Sedimentology **36**(5):*837-855*

Teza G, Galgaro A, Zaltron N, Genevois R (2007) Terrestrial laser scanner to detect landslide displacement fields: a new approach. International Journal of Remote Sensing **28**:*3425-3446*

Trinks I, Clegg P, McCaffrey KJW, Jones RR, Hobbs R, Holdsworth RE, Holliman N, Imber J, Waggot S, Wilson RW (2006) Mapping and analysing virtual outcrops. Visual Geosciences **10**:*13-19*

van Westen CJ, Lulie Getahun F (2003) Analyzing the evolution of the Tessina landslide using aerial photographs and digital elevation models. Geomorphology **54**(1-2):*77-89*

Ventura G, Vilardo G (2008) Emplacement mechanism of gravity flows inferred from high resolution Lidar data: The 1944 Somma-Vesuvius lava flow (Italy). Geomorphology **95**(3-4):*223-235*

Walker GPL (2000) Basaltic volcanoes and volcanic systems. . In: Sigurdsson H (ed) Encyclopedia of Volcanoes. Academic Press San Francisco (CA), pp 283-289

Waters AC, Fisher RV (1971) Base-surges and their deposits: Capelinhos and Taal volcanoes. Journal of Geophysical Research **76**:*5596-5614*

White JDL (1996) Impure coolants and interaction dynamics of phreatomagmatic eruptions. Journal of Volcanology and Geothermal Research **74**(3-4):*155-170*

White JDL, Houghton B (2000) Surtseyan and related phreatomagmatic eruptions. In: Sigurdsson H, Houghton BF, McNutt SR, Rymer H, Stix J (eds) Encyclopedia of Volcanoes. Academic Press, San Diego, pp 495- 511

White JDL, Ross PS (2011) Maar-diatreme volcanoes: A review. Journal of Volcanology and Geothermal Research **201**(1-4):*1-29*

Wohletz KH (1986) Explosive magma-water interactions: Thermodynamics, explosion mechanisms, and field studies. Bulletin of Volcanology **48**:*245-264*

Wong KW (1980) Basic mathematics of photogrammetry. In: Slama CC (ed) Manual of Photogrammetry. American Society of Photogrammetry, Falls Church, VA, pp 37-101

Xu X, Aiken CL, Bhattacharya JP, Corbeanu R, Nielsen KC, McMechan GA, Abdelsalam MG (2000) Creating virtual 3-D outcrop. The Leading Edge **February**:*197–202*

Figure captions

Fig. 1: Example of three monogenetic volcanic edifices with their internal structure exposed by natural and/or anthropogenic (i.e. quarrying) erosional processes. a) Volcano Capelinhos (Faial Island, Azores, Portugal), b) El Golfo volcano (Lanzarote Island, Canary Islands, Spain), c) Croscat volcano (La Garrotxa volcanic field, Spain) (image source: Documentation Centre La Garrotxa Volcanic Field Natural Park, Author: P.Callís).

Fig. 2: a) Principles of laser scanner data acquisition. b) Image of the Terrestrial Laser Scanner equipment used for this study. Additional components such as power supply, GPS and the digital camera are also indicated. c) Sketch of the steps followed to acquire a 3D photo-realistic digital outcrop.

Fig. 3: Screenshot of DigiStruc-3D software during the analysis of the digital outcrop.

Fig. 4: a) Location map of the Catalan Volcanic Zone in the context of European rift systems (modified from Martí et al. 2011). b) Simplified geological map of the Catalan Volcanic Zone and its surroundings (modified from Guérin et al. 1985).

Fig. 5: a) Digital Elevation Model of La Garrotxa Volcanic Field with volcanic cones labelled. b) (top left) Oblique aerial photograph of Croscat volcano showing the location of the study area in the former quarry. (top right) Digital Elevation Model of Santa Margarida, Croscat and La Pomareda volcanoes. (bottom) Oblique aerial photograph of

the Croscat volcano crater and lava flow with the Santa Margarida volcano in the background.

Fig. 6: Image of the southeast-facing scarp of the outcrop under study. A synthetic stratigraphic section of the Croscat volcano is also included (modified from Martí et al. 2011).

Fig. 7: a) Aerial Google Earth image of the Croscat volcano. The extension of the studied outcrop (yellow dashed line) and the position of the three TLS scan points (S1-S3) are indicated. b) Image of the final TLS point cloud once all scans have been merged.

Fig. 8: Rainfall graphs of the La Garrotxa Volcanic Field Natural Park for the individual months during the period 2003-2012 (a) and the total annual accumulated rain (b). Red dashed horizontal line in b) corresponds to the mean value of annual precipitation for the period 2003-2012. Maximum rain during a 24 hours (c) and 30 minutes (d) time period. Data obtained from the Servei Meteorològic Català (http://www.meteo.cat). In case of c) and d) plots, there is no data available for the years 2004-2006.

Fig. 9: Results obtained for difference between DEM_{TLS} - DEM_{ICGC} (in m) for the whole outcrop (a) and specifically for the slope area (b). Pink dashed line in a) indicates the area covered by b). Black background represents those areas where the difference DEM_{TLS} - DEM_{ICGC} could not be estimated due to the lack of information in one or both DEMs.

Fig. 10: Images of the scans where visible stratigraphic layers (green) and contacts (yellow) have been identified. Details of the southeast-facing (a) and northwest-facing (b) sides of the outcrop.

Fig. 11: Images of 3D planes of the southeast-facing (a) and northwest-facing (b) sides of the outcrop extracted with DigiStruc-3D. Visible single stratigraphic layers (green) and contacts (yellow) have been identified. Dip angle for some of the planes are also indicated.

Figure 1

Fig. 1: Example of three monogenetic volcanic edifices with their internal structure exposed by natural and/or anthropogenic (i.e. quarrying) erosional processes. a) Volcano Capelinhos (Faial Island, Azores, Portugal), b) El Golfo volcano (Lanzarote Island, Canary Islands, Spain), c) Croscat volcano (La Garrotxa volcanic field, Spain) (image source: Documentation Centre La Garrotxa Volcanic Field Natural Park, Author: P.Callís).

Figure 2

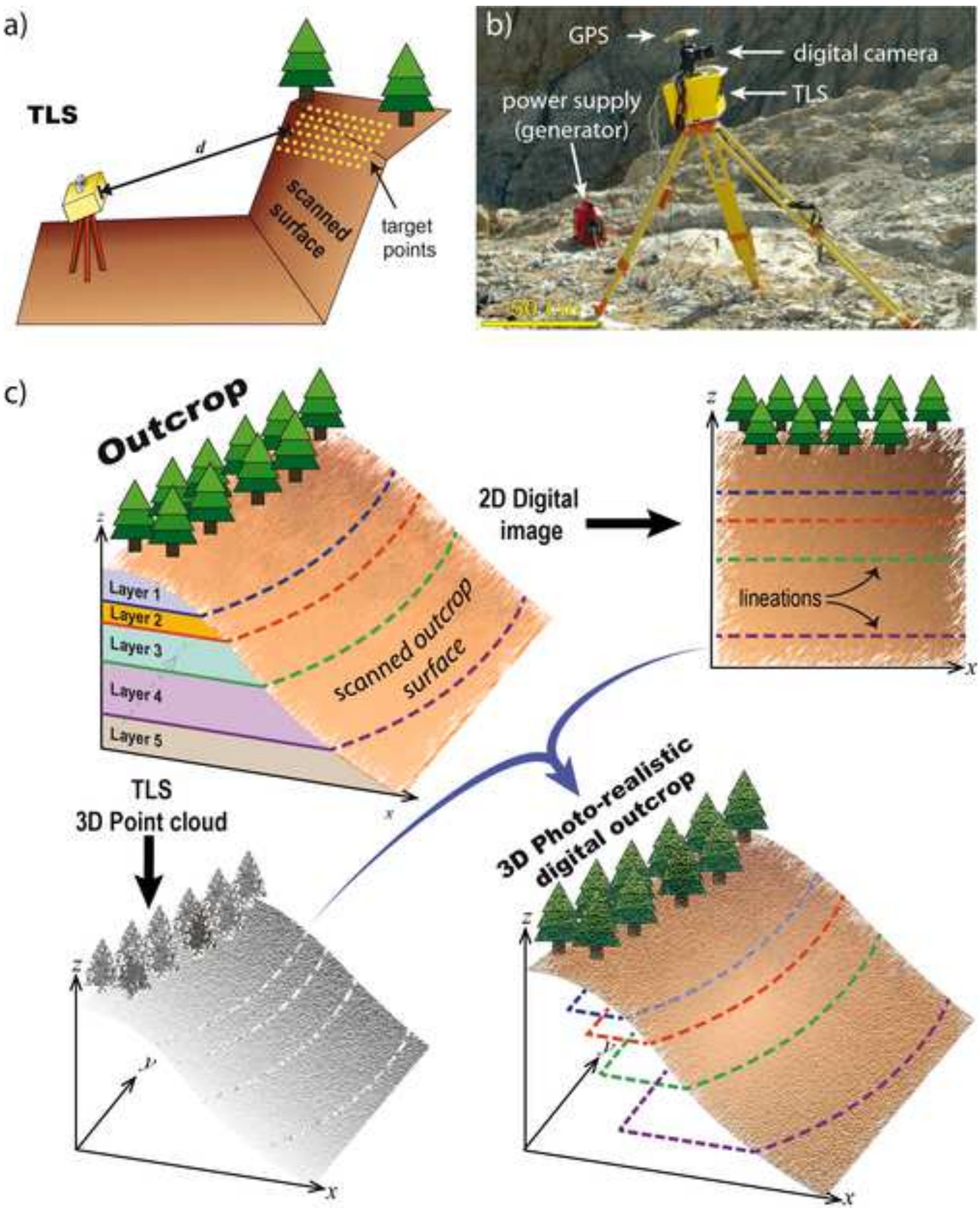

Fig. 2: a) Principles of laser scanner data acquisition. b) Image of the Terrestrial Laser Scanner equipment used for this study. Additional components such as power supply, GPS and the digital camera are also indicated. c) Sketch of the steps followed to acquire a 3D photo-realistic digital

Figure 3

Fig. 3: Screenshot of DigiStruc-3D software during the analysis of the digital outcrop.

Figure 4

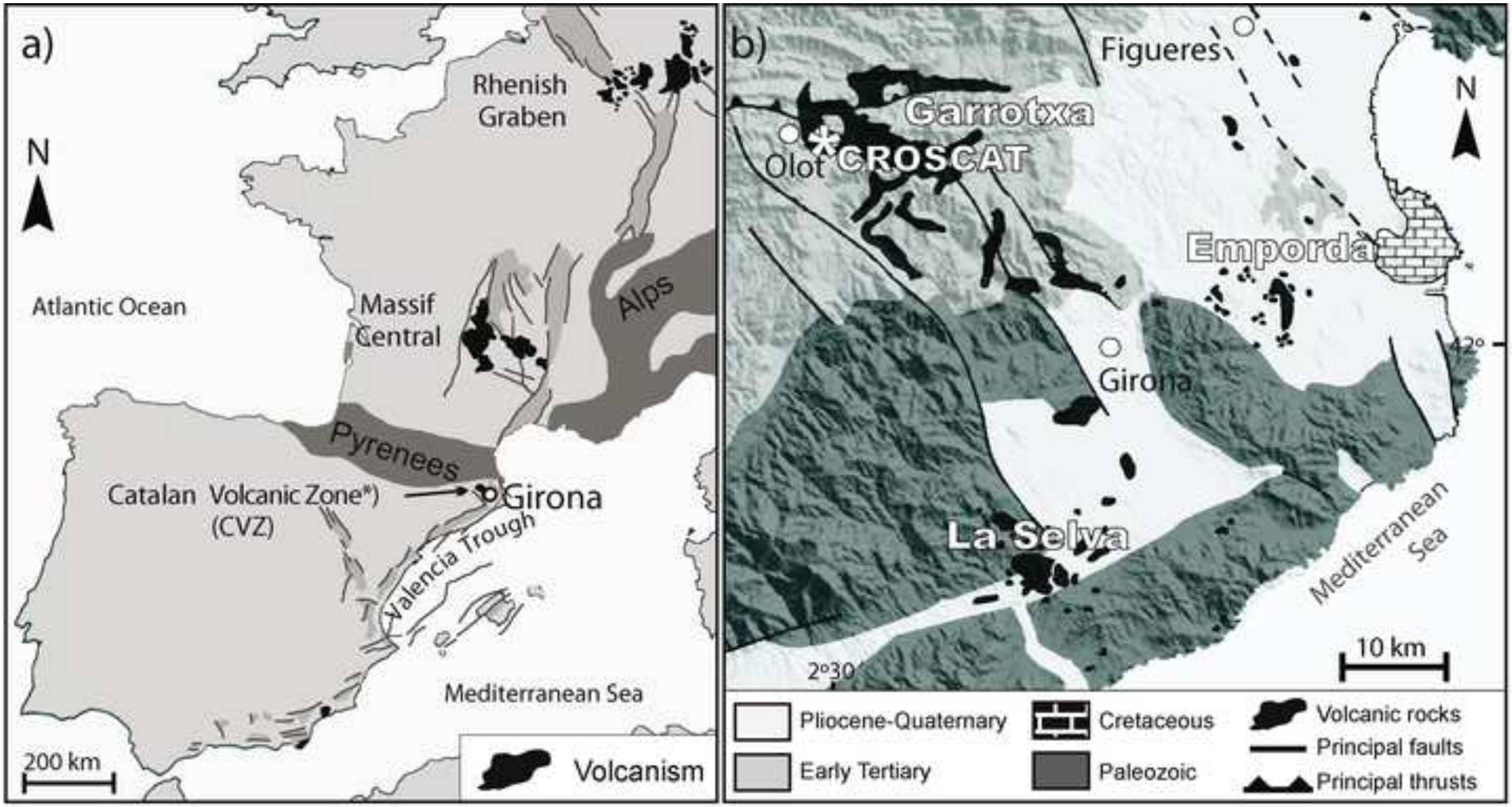

Fig. 4: a) Location map of the Catalan Volcanic Zone in the context of European rift systems (modified from Martí et al. 2011). b) Simplified geological map of the Catalan Volcanic Zone and its surroundings (modified from Guérin et al. 1985).

Figure 5

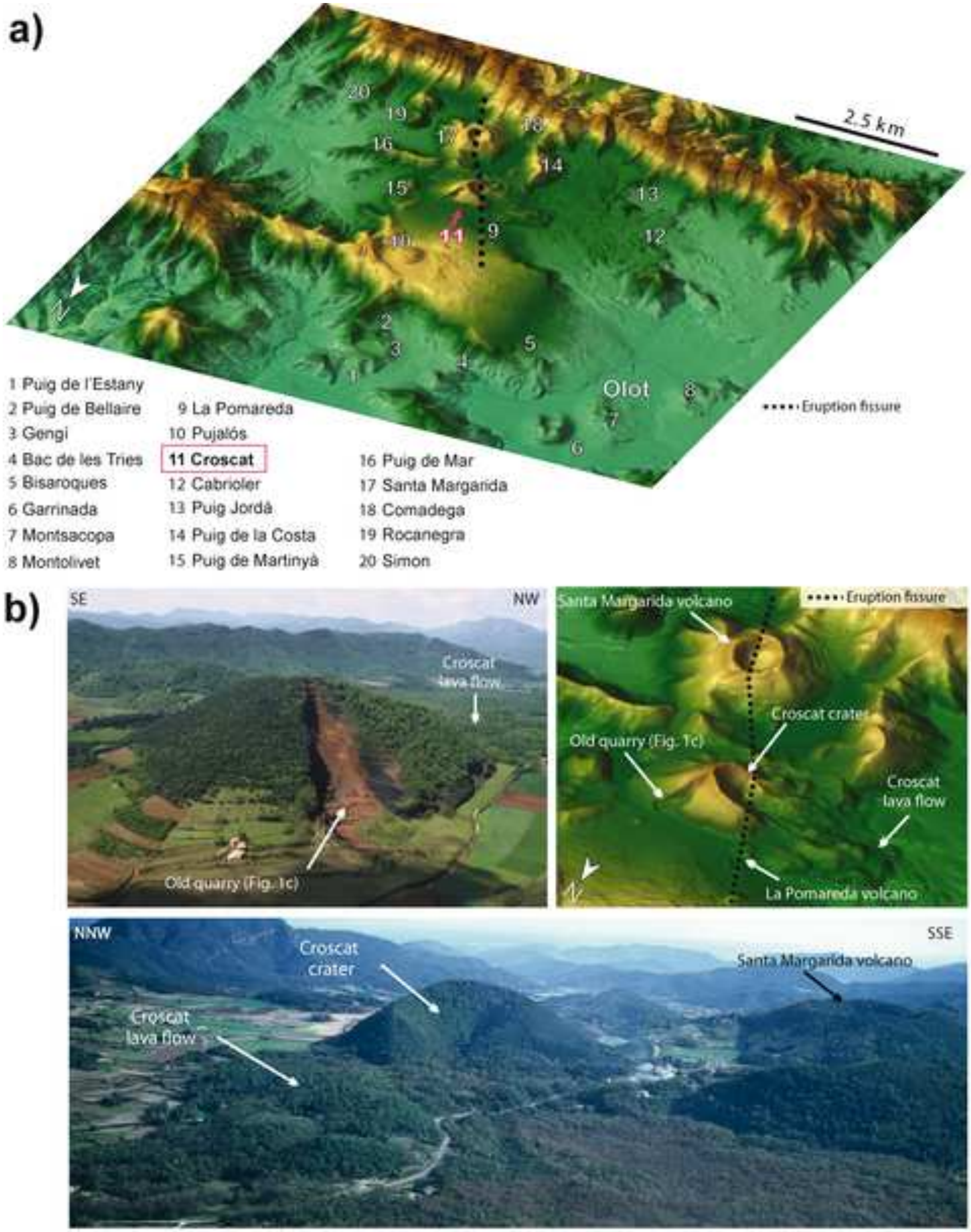

Fig. 5: a) Digital Elevation Model of La Garrotxa Volcanic Field with volcanic cones labelled. b) (top left) Oblique aerial photograph of Croscat volcano showing the creation of the study area in the former quarry. (top right) Digital Elevation Model of Santa Margarida, Croscat and La Pomareda volcanoes. (bottom) Oblique aerial photograph of the Croscat volcano crater and lava flow with the Santa Margarida volcano in the background.

Figure 6

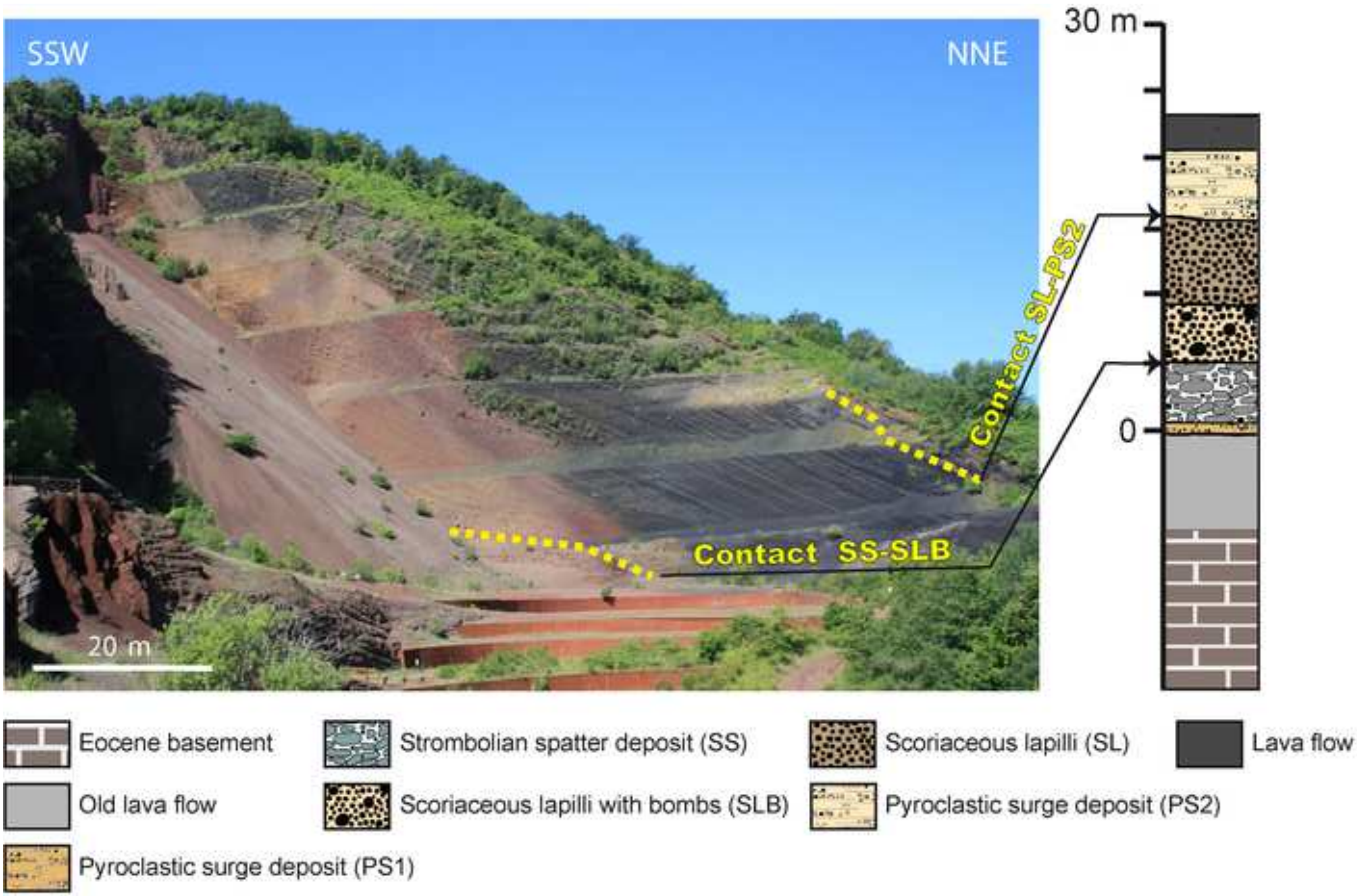

Fig. 6: Image of the southeast-facing scarp of the outcrop under study. A synthetic stratigraphic section of the Croscat volcano is also included (modified from Martí et al. 2011).

Figure 7

a)

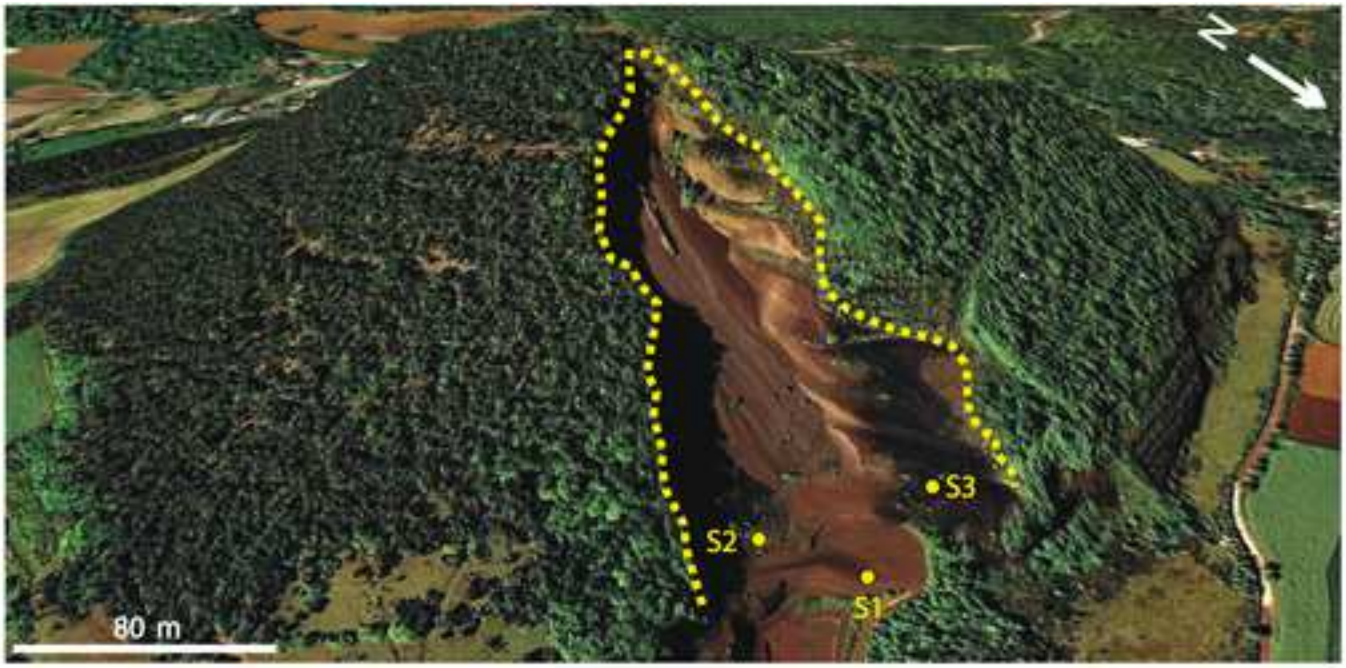

b)

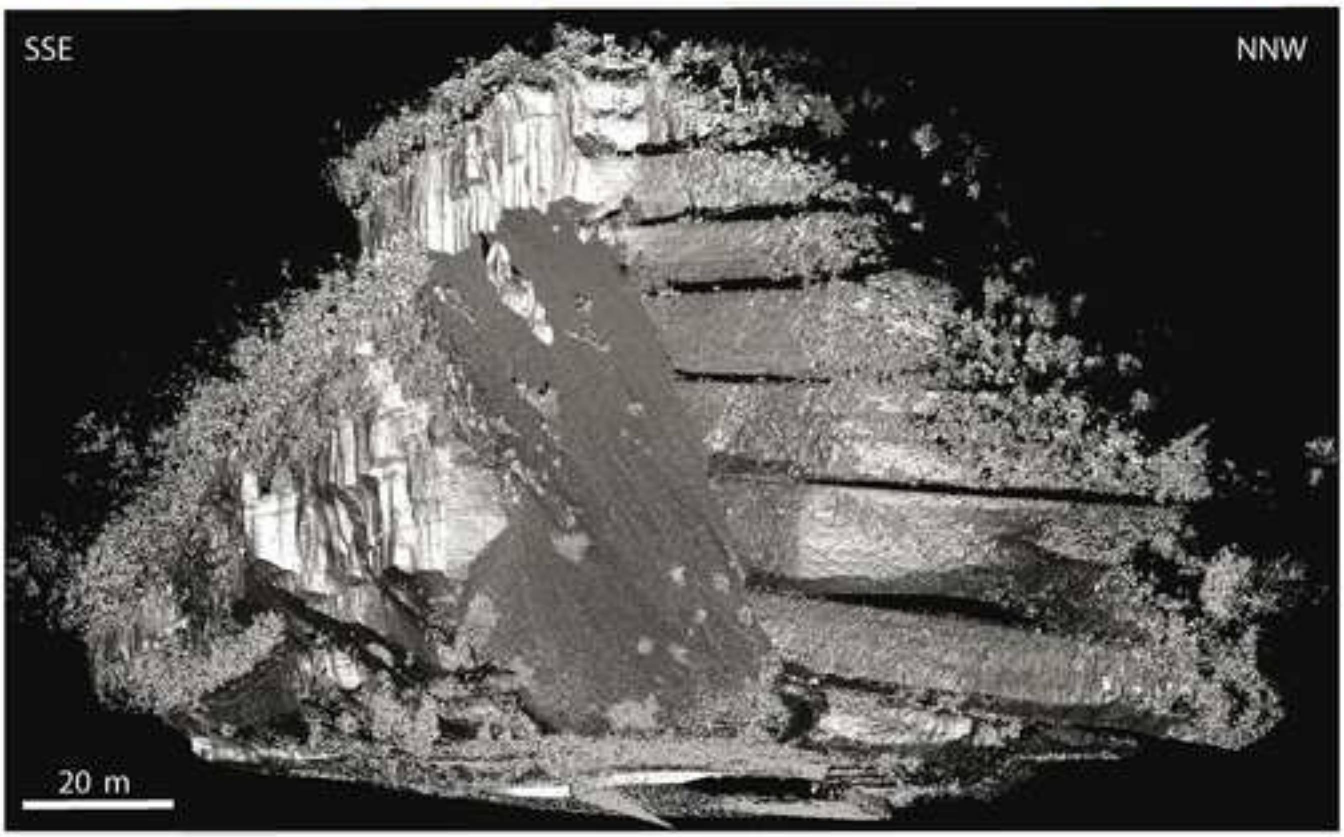

Fig. 7: a) Aerial Google Earth image of the Croscat volcano. The extension of the studied outcrop (yellow dashed line) and the position of the three TLS scan points (S1-S3) are indicated. b) Image of the final TLS point cloud once all scans have been merged.

Figure 8

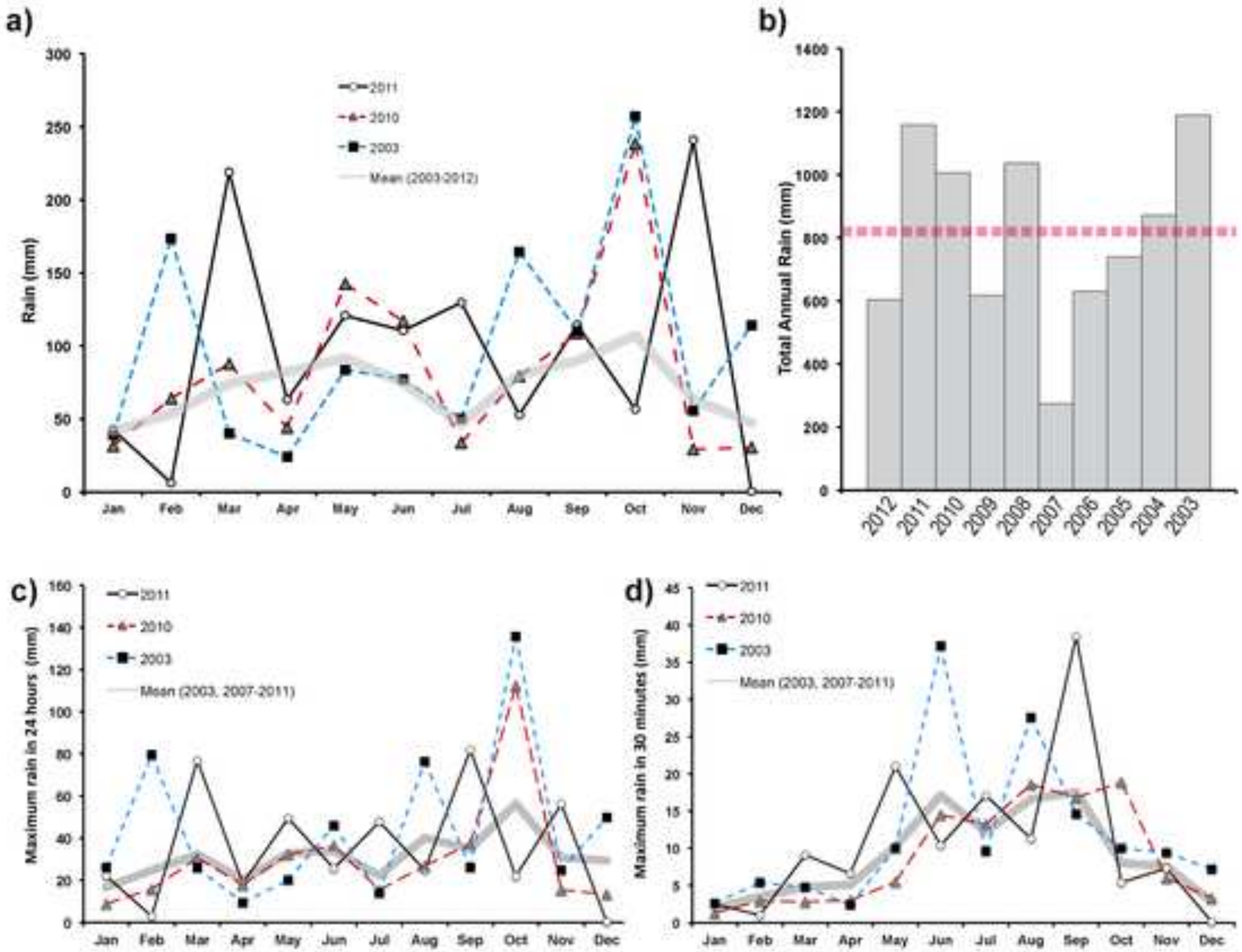

Fig. 8: Rainfall graphs of the La Garrotxa Volcanic Field Natural Park for the individual months during the period 2003-2012 (a) and the total annual accumulated rain (b). Red dashed horizontal line in b) corresponds to the mean value of annual precipitation for the period 2003-2012. Maximum rain during a 24 hours (c) and 30 minutes (d) time period. Data obtained from the Servei Meteorològic Català (http://www.meteo.cat). In case of c) and d) plots, there is no data available for the years 2004-2006.

Figure 9

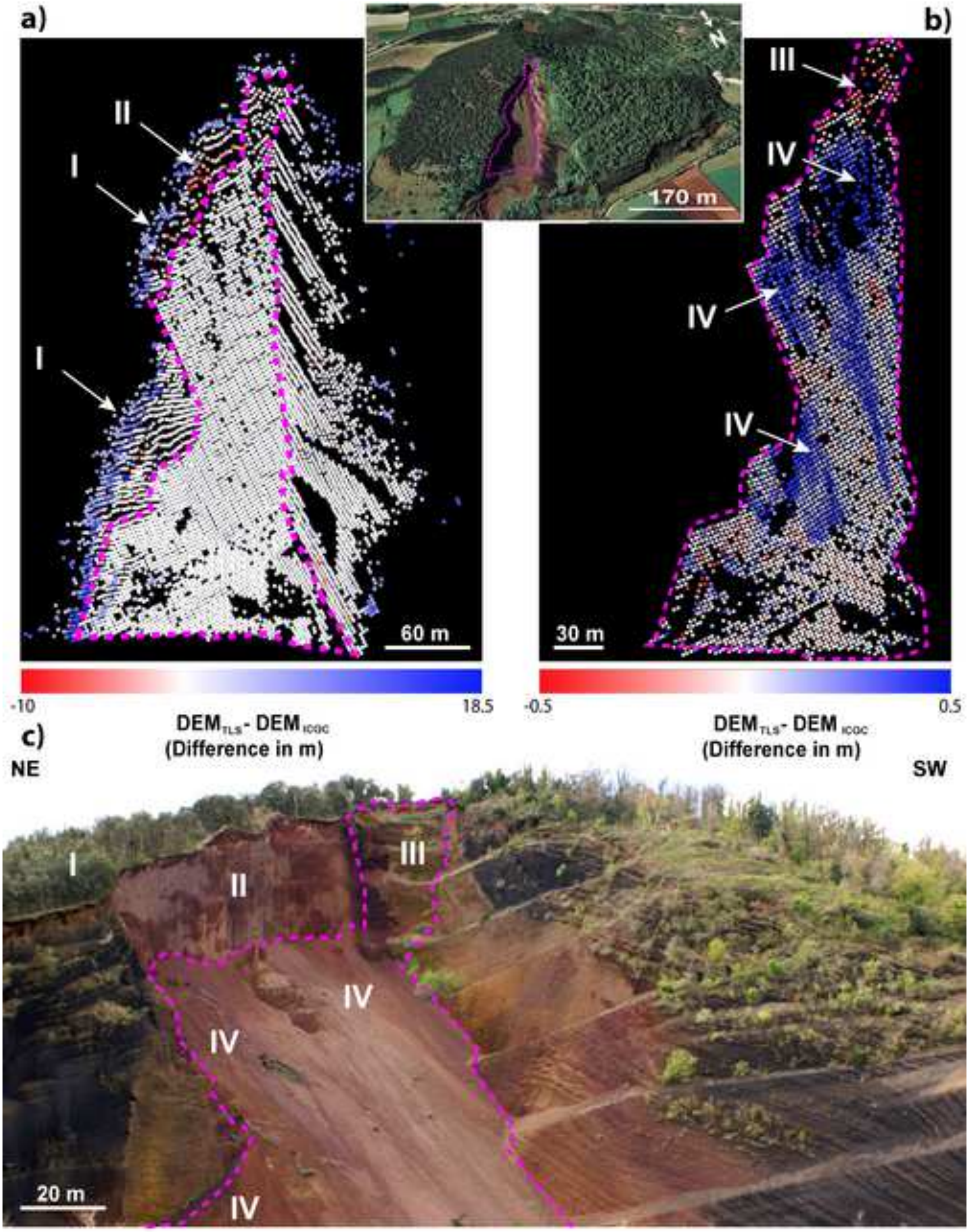

Fig. 9: Results obtained for difference between DEM_{TLS} - DEM_{ICGC} (in m) for the whole outcrop (a) and specifically for the slope area (b). Pink dashed line in a) indicates the area covered by b). Black background represents those areas where the difference DEM_{TLS} - DEM_{ICGC} could not be estimated due to the lack of information in one or both DEMs.

Figure 10

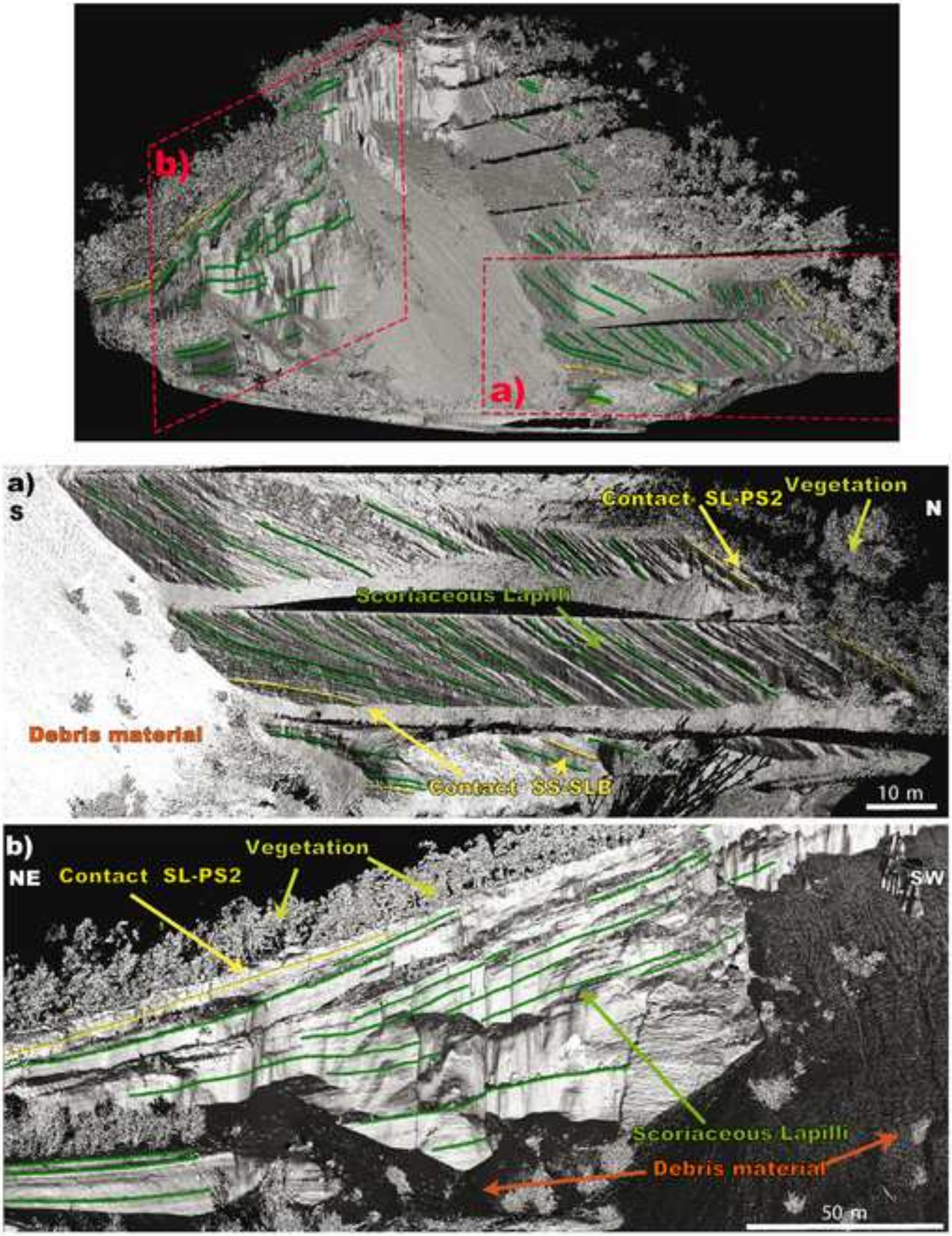

Fig. 10: Images of the scans where visible stratigraphic layers (green) and contacts (yellow) have been identified. Details of the southeast-facing (a) and northwest-facing (b) sides of the outcrop.

Figure 11

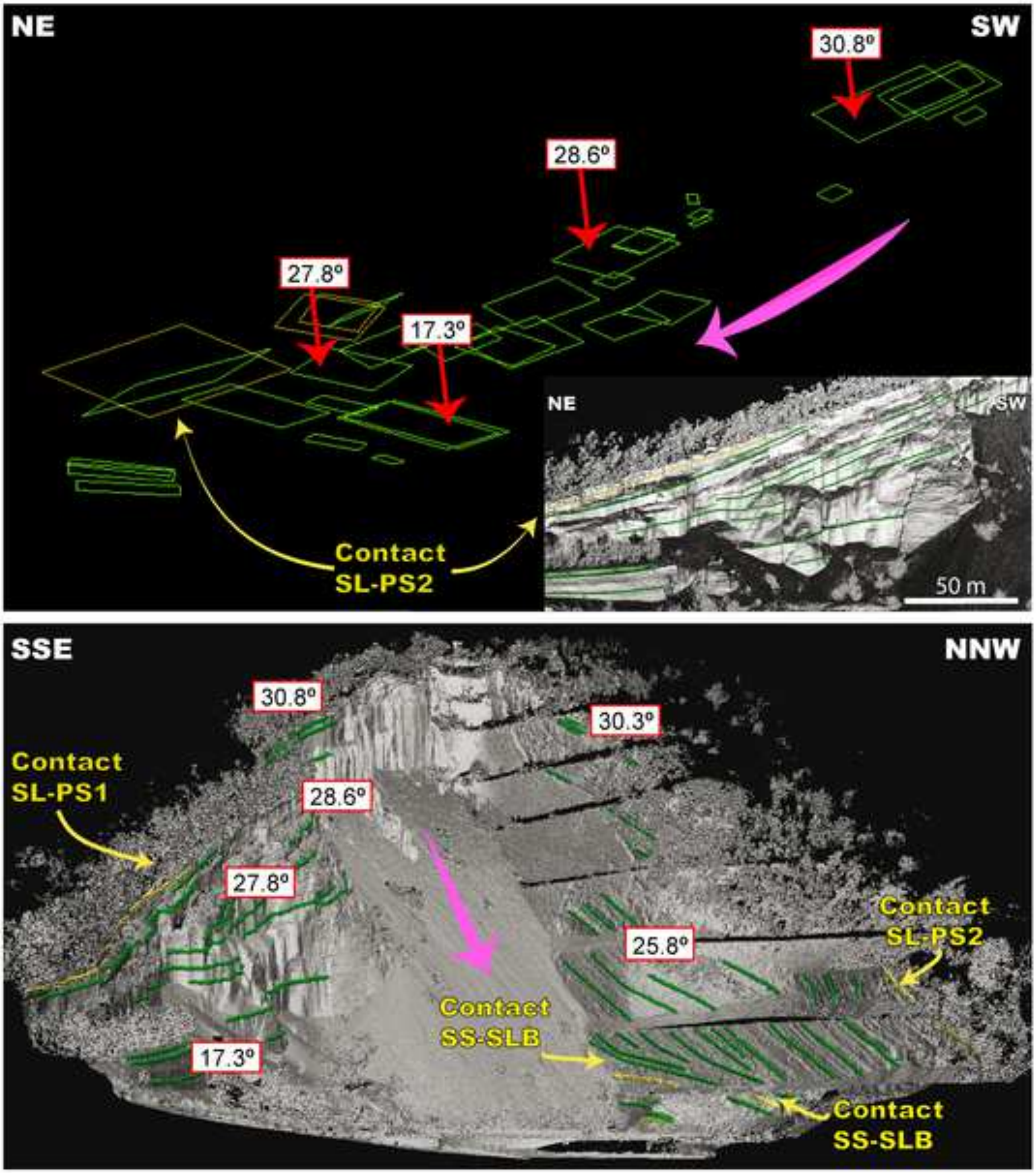

Fig. 11: Images of 3D planes of the southeast-facing (a) and northwest-facing (b) sides of the outcrop extracted with DigiStruc-3D. Visible single stratigraphic layers (green) and contacts (yellow) have been identified. Dip angle for some of the planes are also indicated.